

# NATIONAL ADVISORY COMMITTEE FOR AERONAUTICS

TECHNICAL NOTE 3395

ON THE CALCULATION OF THE 1-P OSCILLATING AERODYNAMIC  
LOADS ON SINGLE-ROTATION PROPELLERS IN PITCH

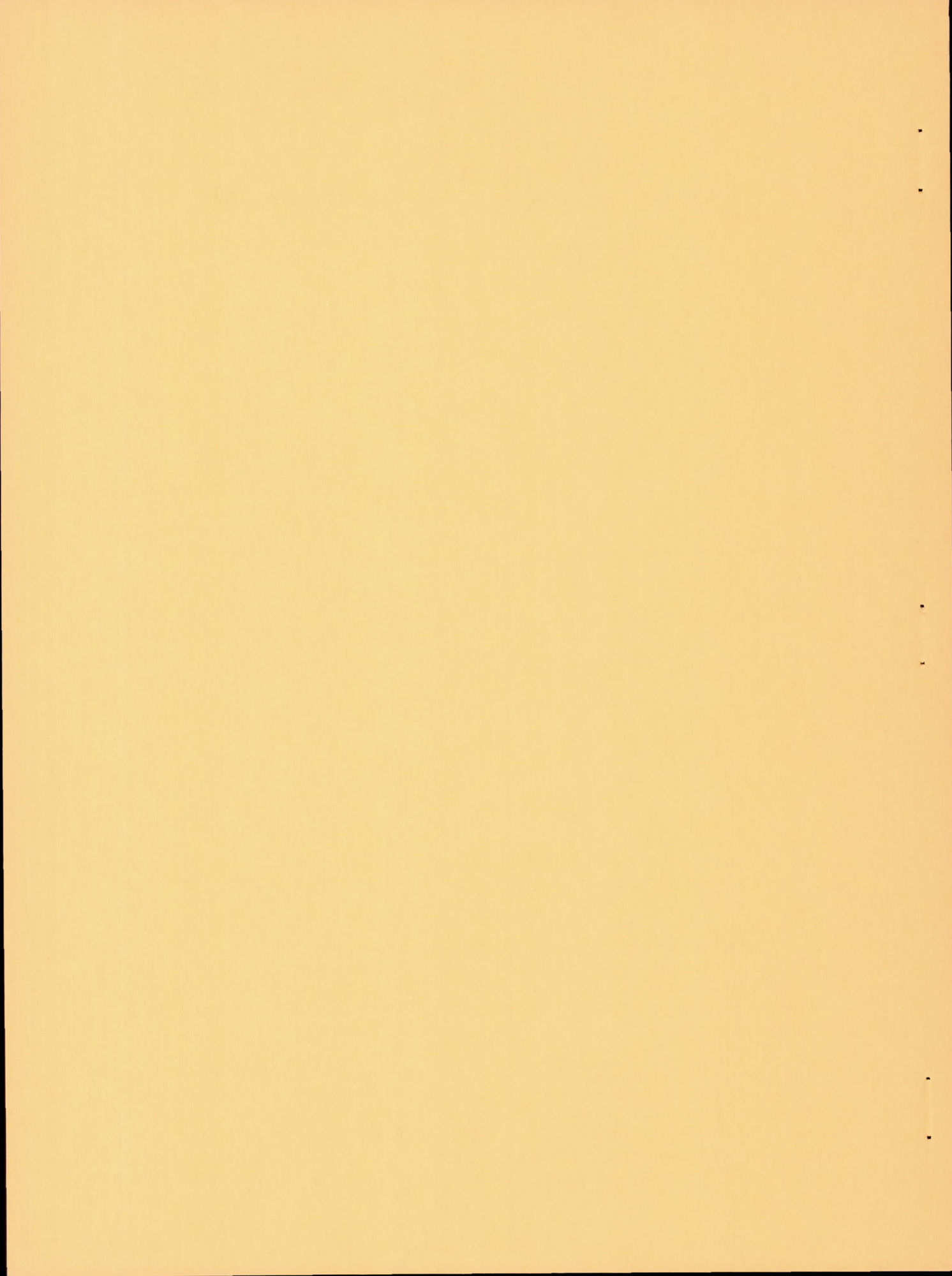
ON TRACTOR AIRPLANES

By Vernon L. Rogallo and Paul F. Yaggy

Ames Aeronautical Laboratory  
Moffett Field, Calif.



Washington  
May 1955



1J  
NATIONAL ADVISORY COMMITTEE FOR AERONAUTICS

---

---

TECHNICAL NOTE 3395

---

ON THE CALCULATION OF THE 1·P OSCILLATING AERODYNAMIC  
LOADS ON SINGLE-ROTATION PROPELLERS IN PITCH  
ON TRACTOR AIRPLANES

By Vernon L. Rogallo and Paul F. Yaggy

SUMMARY

A simplified procedure has been developed to calculate the 1·P oscillating aerodynamic thrust loads on single-rotation propellers in pitch at zero yaw on tractor airplanes. The application of this procedure requires only a knowledge of the upflow angles at the horizontal center line of the propeller disk. These angles may be obtained by computational methods thereby obviating the need for experimental flow surveys.

The 1·P thrust loads and 1·P vibratory stresses computed by the simplified procedure are compared with those calculated using all the flow-field characteristics measured for several wing-nacelle-fuselage combinations. These comparisons show good agreement for the 1·P thrust loads and the 1·P vibratory stresses.

An analysis is included to show the effects of the various flow-field parameters on the 1·P thrust loads.

INTRODUCTION

An important consideration in the design of propellers is that which deals with vibratory stresses which occur one cycle per revolution (commonly referred to as 1·P). These stresses are due to 1·P oscillating aerodynamic thrust loads imposed on propeller blades as a result of propeller thrust-axis inclination and/or asymmetries of the flow fields in which the propellers operate. Currently, the structural design criterion for propeller blades is based upon the allowable amplitudes of the 1·P vibratory stresses. Therefore, there is need for a simple, rapid method of estimating the amplitude of the 1·P thrust loads.

It has been shown in previous work (refs. 1 and 2) that steady-state propeller theory may be applied to predict adequately the oscillating portions of the thrust load on a propeller-blade element around the disk if all the characteristics of the flow field in which it is operating are known. The amplitude of the 1·P component of this variation (the 1·P thrust load) then may be obtained and this load used to determine the 1·P

stresses in the blade. This method is quite laborious, requiring computations for at least 16 points around the disk for each radial position to define accurately the variation of the oscillating thrust load. Further, the characteristics of the entire flow field at present may be obtained only by experimental survey, a cumbersome task which requires considerable time.

This report presents a procedure for calculating the 1·P thrust load by considering only the upflow angles at the horizontal center line of the propeller disk. These angles may be computed theoretically by the methods presented in references 3, 4, and 5, and thus the need for experimental survey is obviated. The procedure is evaluated by comparisons of the 1·P thrust loads computed by the procedure with those computed by a more rigorous method for several wing-nacelle-fuselage combinations.

#### NOTATION

B	number of blades
c	blade chord
$c_t$	blade-section thrust coefficient, $\frac{\text{section thrust}}{\rho n^2 D^4}$
$c_{t_l}$	blade-section thrust coefficient due to section lift force only, $\frac{\text{section thrust due to lift}}{\rho n^2 D^4}$ (See Appendix A.)
$\Delta c_{t_l}$	incremental values of the coefficients, the value at any angular position minus the mean value
D	propeller diameter
K	Goldstein correction factor for a finite number of blades
n	propeller rotational speed
r	distance along any radial line from the propeller thrust axis
R	propeller radius
$v_l$	local velocity at any point $(r, \Omega)$ at the propeller plane (Direction of this velocity is determined by the angles $\theta$ and $\psi$ . See fig. 1.)

$V_o$	free-stream velocity
$V^*$	component of the local velocity in the plane perpendicular to a radial line (See fig. 1.)
$\frac{V_l}{V_o}$	velocity ratio at any point $(r, \Omega)$ at the propeller plane
$x$	radial location of any blade section, $\frac{r}{R}$
$l \cdot P$	the fundamental component (one cycle per propeller revolution) of the oscillation of the section thrust coefficient or of the vibratory blade stresses
$\alpha_G$	geometric angle of attack of the airplane thrust axis
$\alpha_i$	propeller-induced angle of inflow
$\beta$	section blade angle
$\gamma$	$\tan^{-1} \left( \frac{\text{blade-section drag}}{\text{blade-section lift}} \right)$
$\delta_{ctl}$	amplitude of the $l \cdot P$ component of the variation of incremental section thrust coefficient due to section lift force, further defined as the $l \cdot P$ thrust load
$\theta$	angle of outflow, measured from a line parallel to the thrust axis in a plane through the thrust axis (See fig. 1.)
$\theta^*$	angle at which the local velocity at any point on the propeller disk is inclined to the plane perpendicular to the radial line through that point (See fig. 1.)
$\rho$	mass density of air in the free stream
$\sigma$	propeller-blade-element solidity, $\frac{Bc}{2\pi r}$
$\psi$	angle of rotational flow (an apparent, not an actual, rotation) measured from a line parallel to the thrust axis in a plane perpendicular to a radial line (See fig. 1.) (The value of $\psi$ at the horizontal center line of the propeller disk is identical to the upflow angle at that point and corresponds to the notation "A" in ref. 6.)
$\Omega$	angular position about the thrust axis, measured counterclockwise from the upper vertical position as seen from the front

## Subscripts

$\psi$  effects resulting from consideration of variations in  $\psi$  only

$\theta, V_l/V_o$  effects resulting from consideration of variations in  $\theta$  and  $V_l/V_o$  only

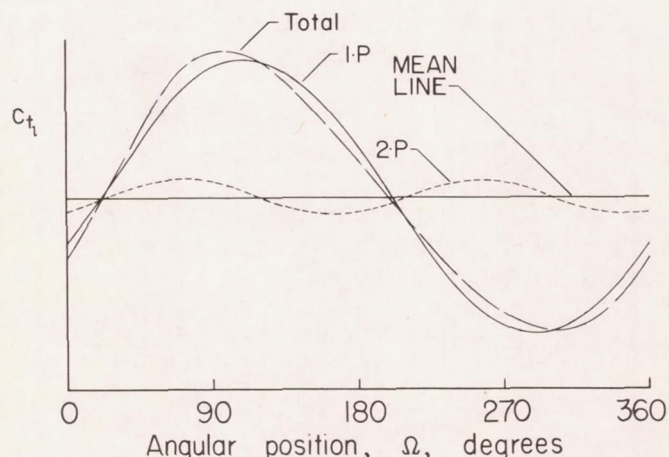
T effects resulting from consideration of variations in  $\psi, \theta$ , and  $V_l/V_o$  acting simultaneously

## PROCEDURE

## Development

Examinations of total oscillating thrust loads for propellers operating in the flow fields of several wing-fuselage-nacelle combinations have indicated a simple procedure for determining the amplitude of the 1·P thrust load. As may be seen in the following sketch of a typical total oscillating thrust load and its harmonic components, no significant odd-order sinusoidal components other than the fundamental (1·P) are present in the variation.<sup>1</sup> The lack of significant higher odd-order components in this variation (and in all other variations examined) makes possible the extraction of the 1·P component of the thrust load by a simple operation which may be applied regardless of the amplitudes or number of even-order components present.

The simplicity of this operation stems from the fact that all even-order harmonics repeat their magnitude and sense at half-cycle intervals of the fundamental; whereas odd-order harmonics, including the fundamental, repeat their magnitude but are of opposite sense at



half-cycle intervals of the fundamental. If the higher odd-order harmonics are nonexistent, one half the arithmetical difference between the values of the total oscillating thrust load at any two angular positions  $180^\circ$  apart (i.e., half-cycle intervals of the fundamental) will yield the exact magnitude of the 1·P component at those points.

---

<sup>1</sup>Harmonic analyses of some of the variations have shown third- and fourth-order components of small amplitude but they are of little significance in the total variation.

The operation may be simplified by utilizing any four equally spaced positions around the propeller disk. For the specific points,  $0^\circ$ ,  $90^\circ$ ,  $180^\circ$ , and  $270^\circ$ , the expressions shown below may be used to determine the amplitude and phase angle of the 1·P component.

$$\frac{1}{2} \left[ \left( c_{t_l} \right)_{\Omega=90^\circ} - \left( c_{t_l} \right)_{\Omega=270^\circ} \right] = \delta c_{t_l} \cos \varphi_a \quad (1)$$

$$\frac{1}{2} \left[ \left( c_{t_l} \right)_{\Omega=0^\circ} - \left( c_{t_l} \right)_{\Omega=180^\circ} \right] = \delta c_{t_l} \sin \varphi_a \quad (2)$$

where

$\delta c_{t_l}$  the amplitude of the 1·P component of thrust load

$\varphi_a$  the angle between the position of the maximum 1·P magnitude and the  $90^\circ$  position.

The small value of  $\varphi_a$  as shown in the foregoing sketch makes plausible the approximation

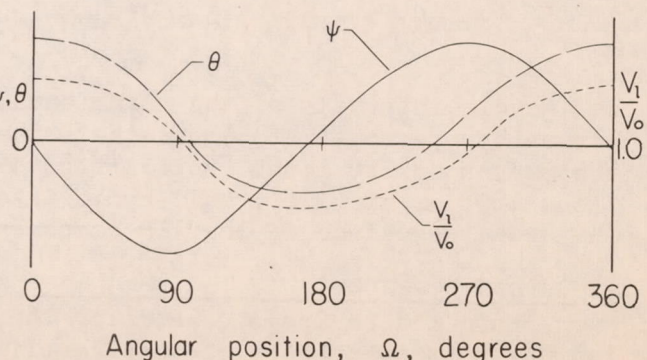
$$\delta c_{t_l} \cos \varphi_a \approx \delta c_{t_l}$$

hence, only the value of  $c_{t_l}$  for the  $90^\circ$  and  $270^\circ$  positions would be required. The procedure then consists of the solution of equation (1) rewritten to include the foregoing approximation, as follows:

$$\frac{1}{2} \left[ \left( c_{t_l} \right)_{\Omega=90^\circ} - \left( c_{t_l} \right)_{\Omega=270^\circ} \right] = \delta c_{t_l} \quad (3)$$

While it is necessary to know the values of all of the flow parameters at these points to calculate the corresponding values of  $c_{t_l}$ , certain characteristics of the flow-field parameters make possible further simplifications. It is seen in the sketch that at the  $90^\circ$  and  $270^\circ$  positions,  $\theta$  and  $V_l/V_o$  are near  $0^\circ$  and 1.0, respectively, while  $\psi$  is near its minimum and maximum values. Thus, the values of  $\theta$  and  $V_l/V_o$  may be approximated as  $0^\circ$  and 1.0, respectively. Since the values of  $\psi$  at these positions

may be computed by methods described in references 3 to 6, experimental survey of the flow field would be unnecessary.



It may occur to the reader to circumvent the approximation

$$\delta c_{t_l} \cos \varphi_a \approx \delta c_{t_l}$$

by utilizing expression (2) and the flow-field characteristics at the  $0^\circ$  and  $180^\circ$  positions. However, it has been found that higher odd-order components which are insignificant in the total  $c_{t_l}$  variation did not greatly affect the accuracy of expression (1), but their presence did greatly affect the accuracy of expression (2) for the small phase angles  $\varphi_a$  involved. The simultaneous solution of expressions (1) and (2) with complete flow-field data did not give greater accuracy than the procedure to be examined in this report.

#### Evaluation

As a means of indicating the accuracy and general applicability of the procedure, 1-P thrust loads computed by the use of this procedure were compared with those determined by a 16-point solution. Measured flow-field data were used for the 16-point solution.<sup>2</sup> For the procedure, measured values of  $\psi$  were used and the values of  $\theta$  and  $V_l/V_o$  were assumed to be  $0^\circ$  and 1.0, respectively. The blade stresses (due to aerodynamic loading alone) resulting from the 1-P thrust loads computed by the two methods were also compared. The geometries of the model configurations considered in these comparisons are shown in figure 2. For purposes of this evaluation, it was assumed that a four-bladed right-hand propeller was installed on each model. The characteristics of this propeller and the method employed in the computation of the stresses are given in reference 1.

The 1-P thrust loads for the 0.7-radial station of the propeller blade for all models as computed by the two methods are compared in figure 3. Comparisons of the radial variations of the 1-P thrust loads computed by both methods for two models are shown in figure 4. The 1-P blade stresses for these two models are shown in figure 5. From these figures, it is seen that the procedure is generally satisfactory.

#### DISCUSSION

Although the procedure of this report may be considered sufficiently accurate for the configurations investigated, it was concluded that it

---

<sup>2</sup>The values of the flow parameters used in these computations were determined by experimental survey and were reported in references 2, 3, and 6. Since data were obtained at the port propeller planes, the flow fields for the starboard propellers were assumed to be the reflected images of those for the port propeller.

would be impossible from a cursory examination of a configuration to predict whether this accuracy could always be realized. To gain an insight into the cause or causes of the 1-P thrust loads, it was decided to investigate the separate effects of the various flow-field parameters. Therefore, the variations of the total thrust loads on a blade element were calculated for the models in the following manner: (1) using measured values of  $\psi$ , and assuming  $\theta = 0^\circ$  and  $V_l/V_o = 1.0$ , (2) using measured values of  $\theta$  and  $V_l/V_o$  and assuming  $\psi = 0^\circ$ , (3) using measured values of  $\psi$ ,  $\theta$ , and  $V_l/V_o$ . From these variations, the 1-P components were extracted. As may be seen from figure 1, the first case shows the effect of the angular variation of the inflow velocity  $V^i$ , while the second case shows the effect of the magnitude variation of the inflow velocity  $V^i$ . While it is not apparent from the equations for the total thrust variations (see Appendix A) that this method would yield the exact effects of the variables, it was found that the summation of the thrust loads for cases (1) and (2) was nearly identical with the thrust variation calculated for case (3). The 1-P components of thrust variations and the associated flow-field parameters are shown in figure 6.

From these figures, it is seen that  $\psi$  produced a 1-P component which peaked at approximately  $90^\circ$  and  $270^\circ$ . Since the procedure of this report utilizes only  $\psi$  at the  $90^\circ$  and  $270^\circ$  positions, it essentially determines the 1-P thrust load due to  $\psi$ . From these figures, it is also seen that  $\theta$  and  $V_l/V_o$  produce a significant 1-P component which peaked at approximately  $0^\circ$  and  $180^\circ$ . The models which have a large 1-P component due to  $\theta$  and  $V_l/V_o$  are characterized by a relatively large blunt nacelle. Further, when the nacelle is mounted on the wing, the magnitudes of these 1-P components are increased due to the velocity gradient induced by the wing. It should be noted, however, that all of these 1-P components due to  $\theta$  and  $V_l/V_o$  are so phased as to add little to the total 1-P component. The total 1-P component appears to be more dependent on the phase angle between the 1-P components due to  $\psi$  and  $\theta$  and  $V_l/V_o$  than on the magnitude of the 1-P component due to  $\theta$  and  $V_l/V_o$ .

Although the foregoing analysis has shown the causes of the 1-P thrust load, the inability to predict the phase angles involved makes it impractical to use this analysis to attempt refinement of the basic procedure of this report. The analysis may prove useful for estimation of probable accuracies of the basic procedure for other configurations.

#### CONCLUDING REMARKS

A procedure has been presented for calculating the 1-P thrust load on propellers of tractor airplanes in pitch at zero yaw, whose application requires only a knowledge of the upflow angles at the horizontal center line of the propeller disk. The evaluation of the procedure showed that the 1-P thrust loads and the 1-P blade stresses resulting

therefrom could be predicted for the airplane configurations investigated and it is believed satisfactory results could be obtained for similar configurations.

Ames Aeronautical Laboratory  
National Advisory Committee for Aeronautics  
Moffett Field, Calif., Mar. 21, 1955

## APPENDIX A

The 1-P stress problem is primarily flatwise bending of the blade which results from oscillations in the blade normal force. Therefore, it is the sum of the components of the thrust and torque forces perpendicular to the chord line of the blade element which must be determined. The normal forces on a blade element may be expressed as

$$N_b = t \cos \beta + f_q \sin \beta \quad (A1)$$

where

$t$  section thrust

$f_q$  section torque force

The section thrust on a blade element was given in coefficient form in reference 2 as

$$c_t = K\pi^3 x^3 \frac{\alpha_i}{57.3} \frac{(\cot \varphi - \tan \gamma)}{\left(\cot \varphi + \frac{\alpha_i}{57.3}\right)^2} \left(1 - \frac{V^* \sin \psi}{\pi n D x}\right)^2 \quad (A2)$$

where

$$\varphi = \varphi_o + \alpha_i$$

$$\varphi_o = \tan^{-1} \left( \frac{V^* \cos \psi}{\pi n D x - V^* \sin \psi} \right)$$

This expression may be simplified to consider only the section thrust due to lift.

$$c_{t_l} = K\pi^3 x^3 \frac{\alpha_i}{57.3} \frac{\cot \varphi}{\left(\cot \varphi + \frac{\alpha_i}{57.3}\right)^2} \left(1 - \frac{V^* \sin \psi}{\pi n D x}\right)^2 \quad (A3)$$

This is the expression which was used to calculate the values of  $c_{t_l}$  considering all the flow-field parameters as measured values. The values of  $0^\circ$  and 1.0 may be substituted for  $\theta$  and  $V_l/V_o$  in this expression as described in the text. The resulting expression is

$$c_{t_l} = K\pi^3 x^3 \frac{\alpha_1}{57.3} \frac{\cot \varphi}{\left(\cot \varphi + \frac{\alpha_1}{57.3}\right)^2} \left(1 - \frac{V_0 \sin \psi}{\pi n D x}\right)^2$$

where

$$\varphi = \varphi_0 + \alpha_1$$

$$\varphi_0 = \tan^{-1} \left( \frac{V_0 \cos \psi}{\pi n D x - V_0 \sin \psi} \right)$$

If the blade normal force is expressed in coefficient form and both section thrust and section torque force are expressed in terms of section thrust due to lift,  $\varphi$ , and  $\gamma$ , equation (A1) becomes

$$c_{N_b} = c_{t_l} \left(1 - \frac{\tan \gamma}{\cot \varphi}\right) \cos \beta + c_{t_l} \left(1 - \frac{\tan \gamma}{\cot \varphi}\right) \tan(\varphi + \gamma) \sin \beta \quad (A4)$$

When equation (4) is rearranged

$$c_{N_b} = \frac{c_{t_l}}{\cos \beta} \left\{ \frac{\cos[(\gamma - \varphi) - 2(\beta - \varphi)] + \cos(\gamma + \varphi)}{\cos(\gamma - \varphi) + \cos(\gamma + \varphi)} \right\} \quad (A5)$$

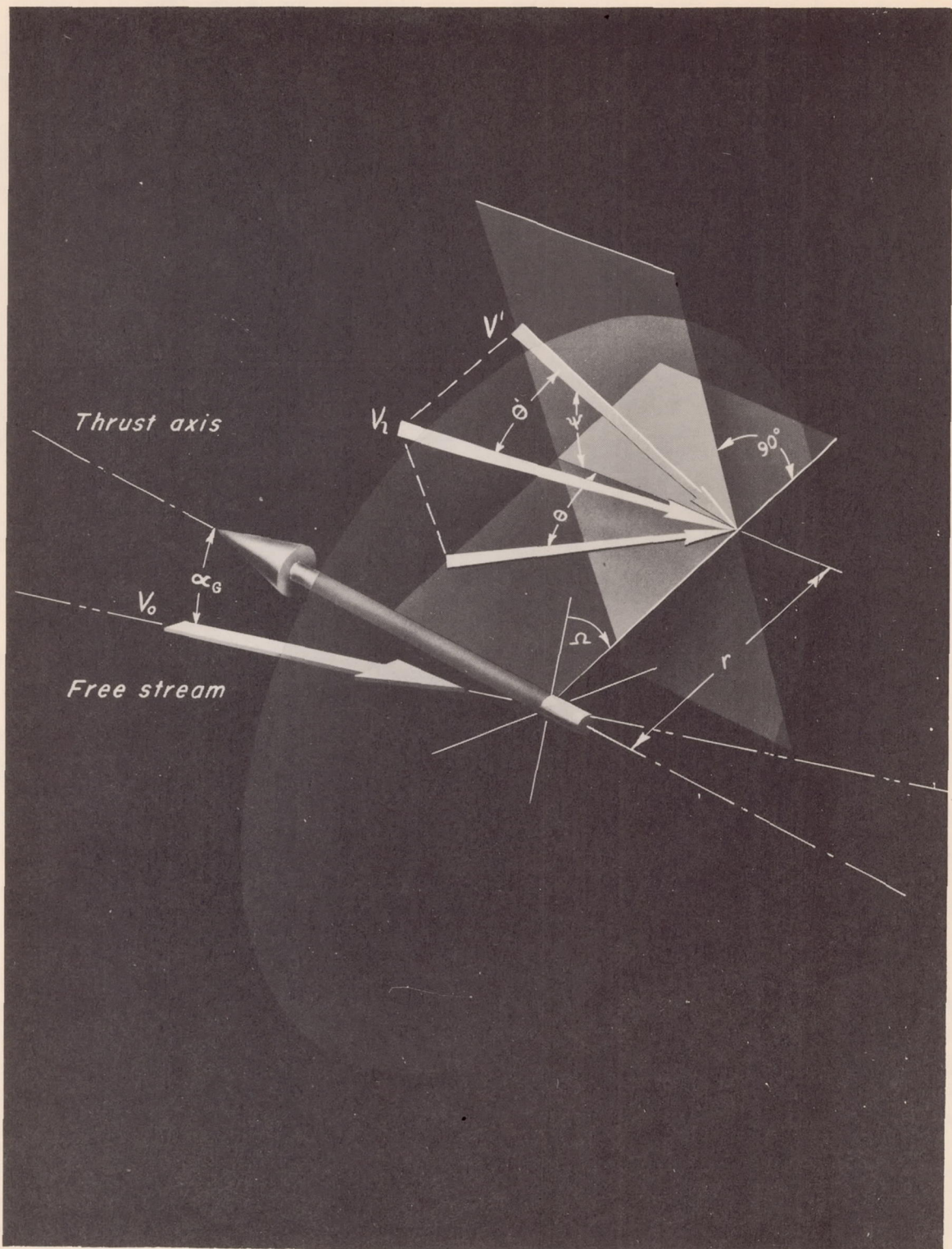
For simplicity, the term in the brackets was assumed to be unity which is tantamount to saying that the drag force on a blade element does not contribute materially to the blade-element normal force. Therefore, only the thrust due to lift on the blade element was considered to obtain the normal force which is expressed as

$$c_{N_b} \approx \frac{c_{t_l}}{\cos \beta}$$

## REFERENCES

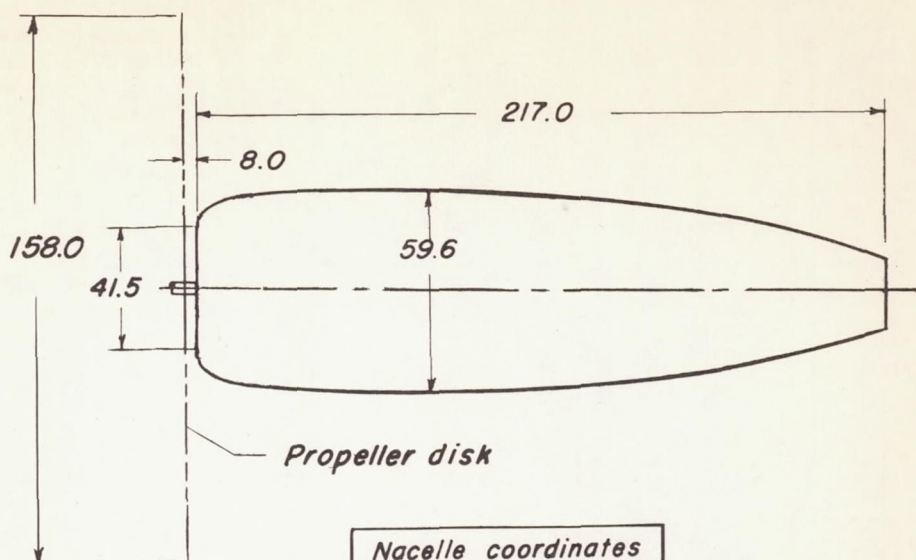
1. Rogallo, Vernon L., Roberts, John C., and Oldaker, Merritt R.: Vibratory Stresses in Propellers Operating in the Flow Field of a Wing-Nacelle-Fuselage Combination. NACA TN 2308, 1951.
2. Roberts, John C., and Yaggy, Paul F.: A Survey of the Flow at the Plane of the Propeller of a Twin-Engine Airplane. NACA TN 2192, 1950.
3. Yaggy, Paul F.: A Method for Predicting the Upwash Angles Induced at the Propeller Plane of a Combination of Bodies With an Unswept Wing. NACA TN 2528, 1951.
4. Rogallo, Vernon L.: Effects of Wing Sweep on the Upwash at the Propeller Planes of Multiengine Airplanes. NACA TN 2795, 1952.
5. Rogallo, Vernon L., and McCloud, John L., III: Calculations of Upwash in the Region Above or Below the Wing-Chord Planes of Swept-Back Wing-Fuselage-Nacelle Combinations. NACA TN 2894, 1953.
6. Rogallo, Vernon L., and McCloud, John L., III: Surveys of the Flow Fields at the Propeller Planes of Six 40° Sweptback Wing-Fuselage-Nacelle Combinations. NACA TN 2957, 1953.





A-14137.2

Figure 1.- Schematic representation of the flow field parameters.



Nacelle coordinates	
Station	Radius
0	21.5
1	23.0
2	24.0
4	25.0
6	26.0
9	27.0
12	27.8
18	28.5
24	29.0
30	29.5
36	29.6
42	29.7
48	29.8
54	29.8
62	29.8
72	29.8
96	29.5
120	29.0
144	26.5
168	22.4
192	16.4
217	11.2

All dimensions are in inches.

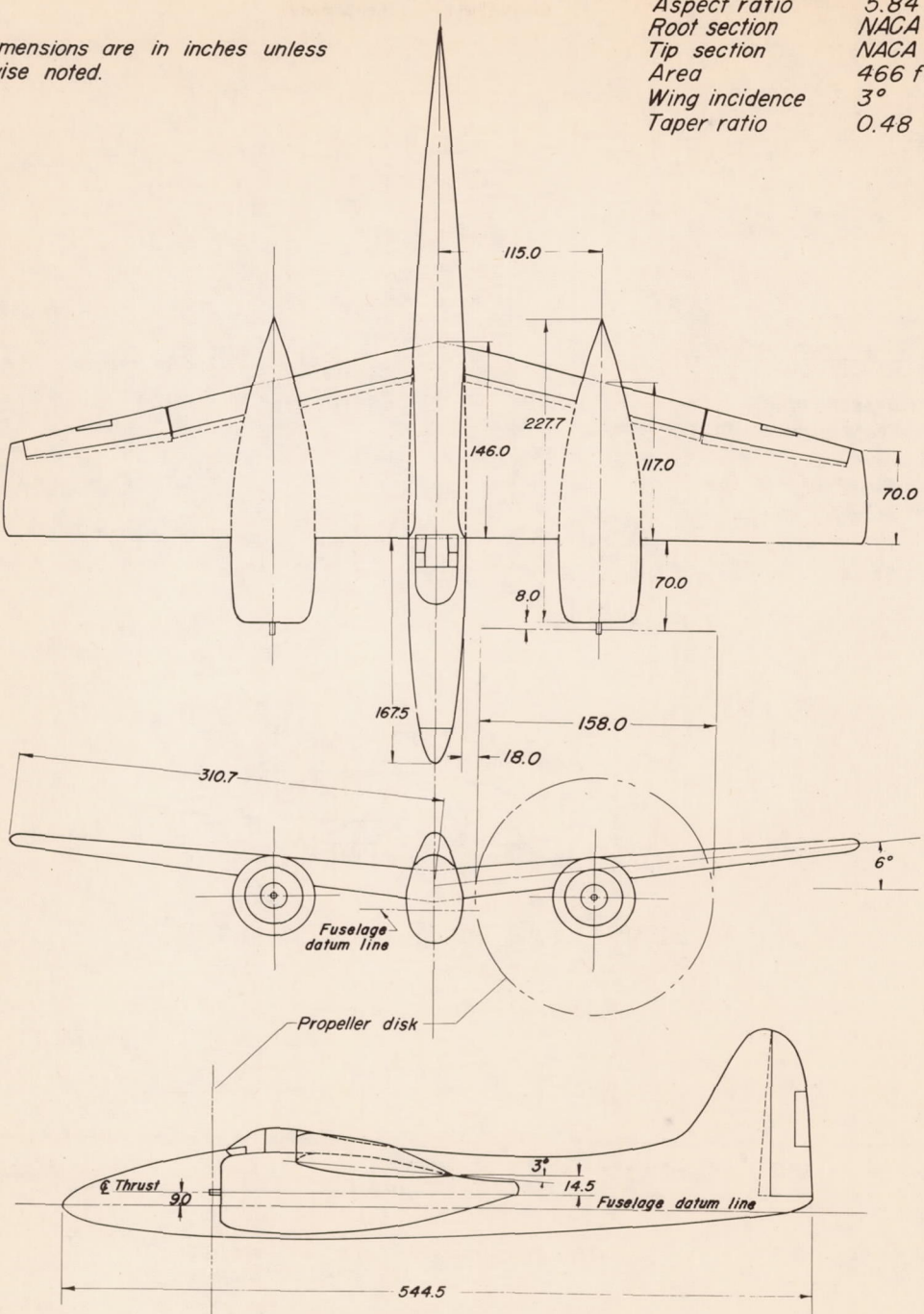
(a) Model a

Figure 2.- Geometric characteristics of the models.

All dimensions are in inches unless otherwise noted.

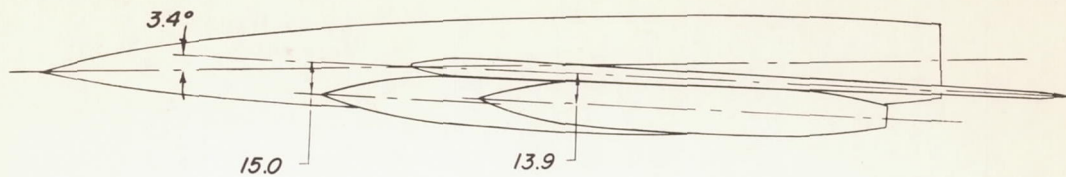
### Wing characteristics

Wing characteristics	
Aspect ratio	5.84
Root section	NACA 23015
Tip section	NACA 23012
Area	466 ft. <sup>2</sup>
Wing incidence	3°
Taper ratio	0.48



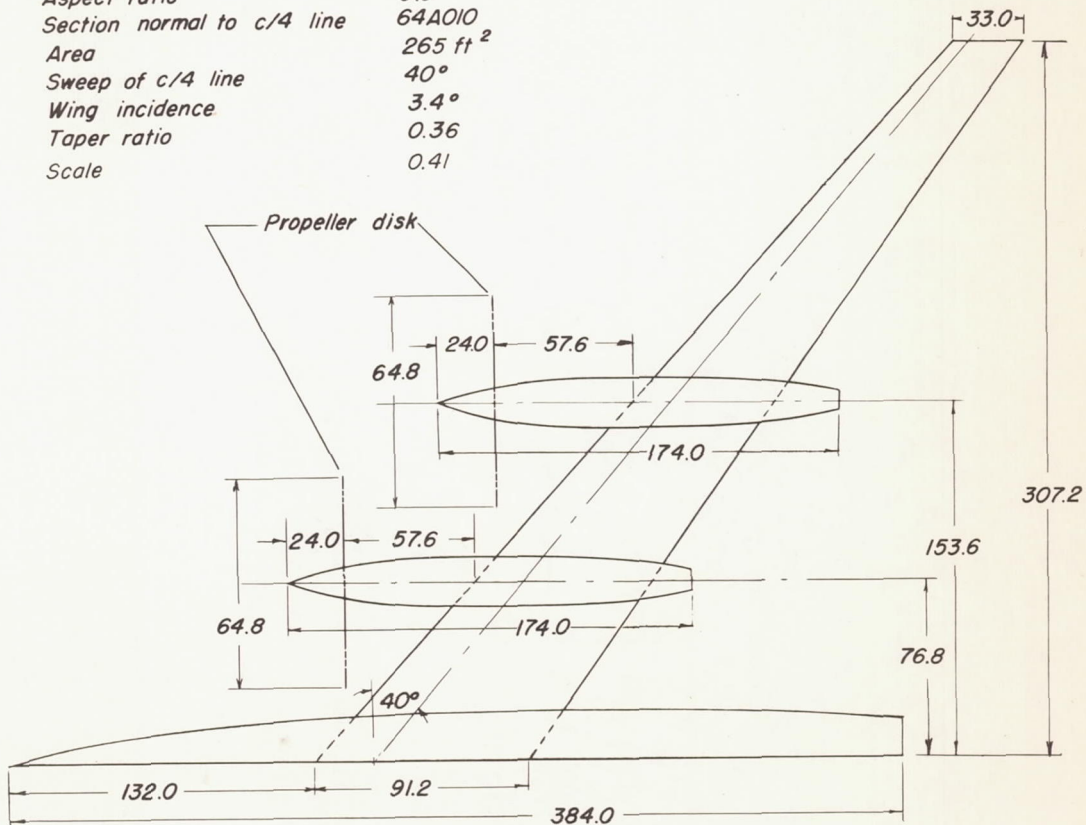
(b) Model b  
Figure 2.—Continued.

All dimensions are in inches



Wing characteristics

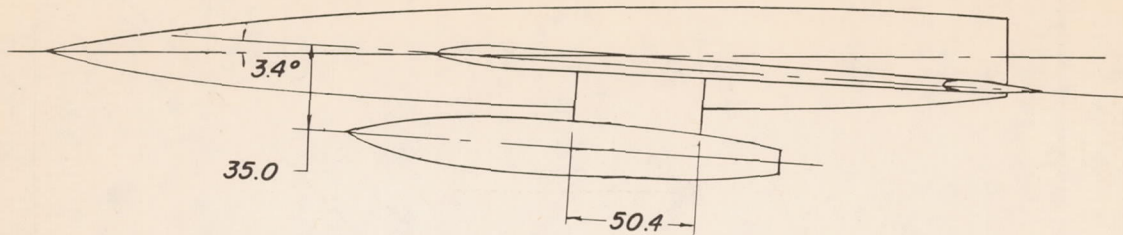
Aspect ratio	9.9
Section normal to c/4 line	64AO10
Area	265 ft <sup>2</sup>
Sweep of c/4 line	40°
Wing incidence	3.4°
Taper ratio	0.36
Scale	0.41



(c) Model c

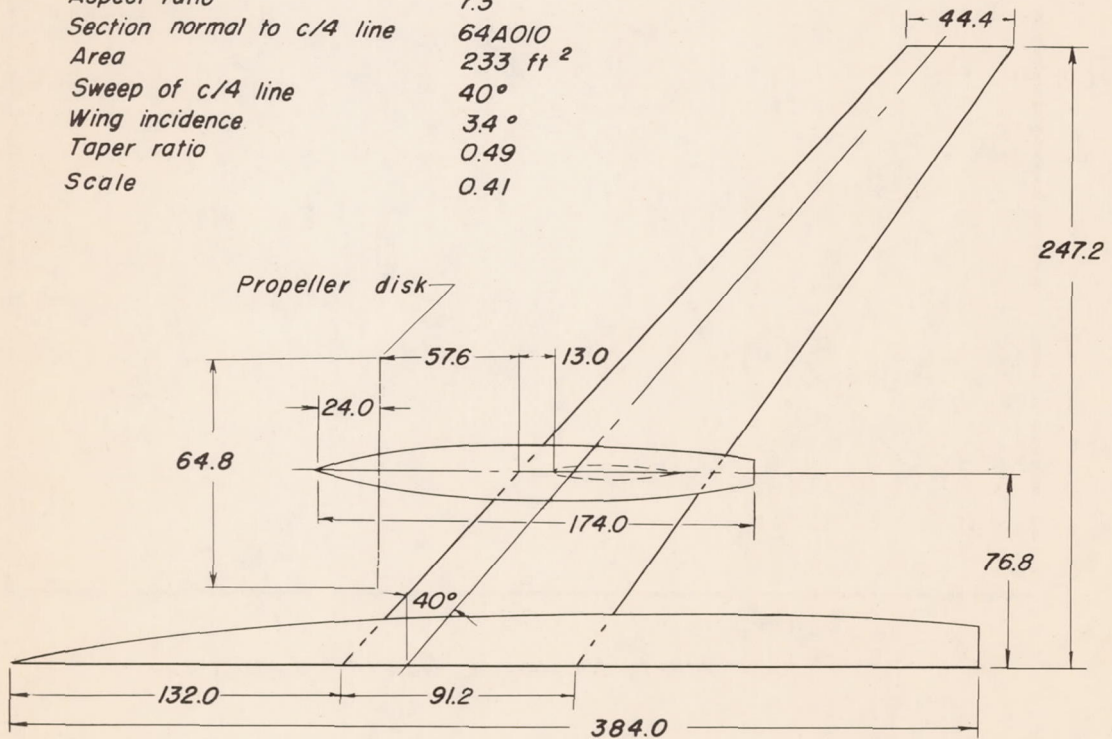
Figure 2.—Continued.

*All dimensions are in inches*



Wing characteristics

Aspect ratio	7.3
Section normal to c/4 line	64A010
Area	233 ft <sup>2</sup>
Sweep of c/4 line	40°
Wing incidence	3.4°
Taper ratio	0.49
Scale	0.41



(d) Model d

Figure 2.—Concluded.

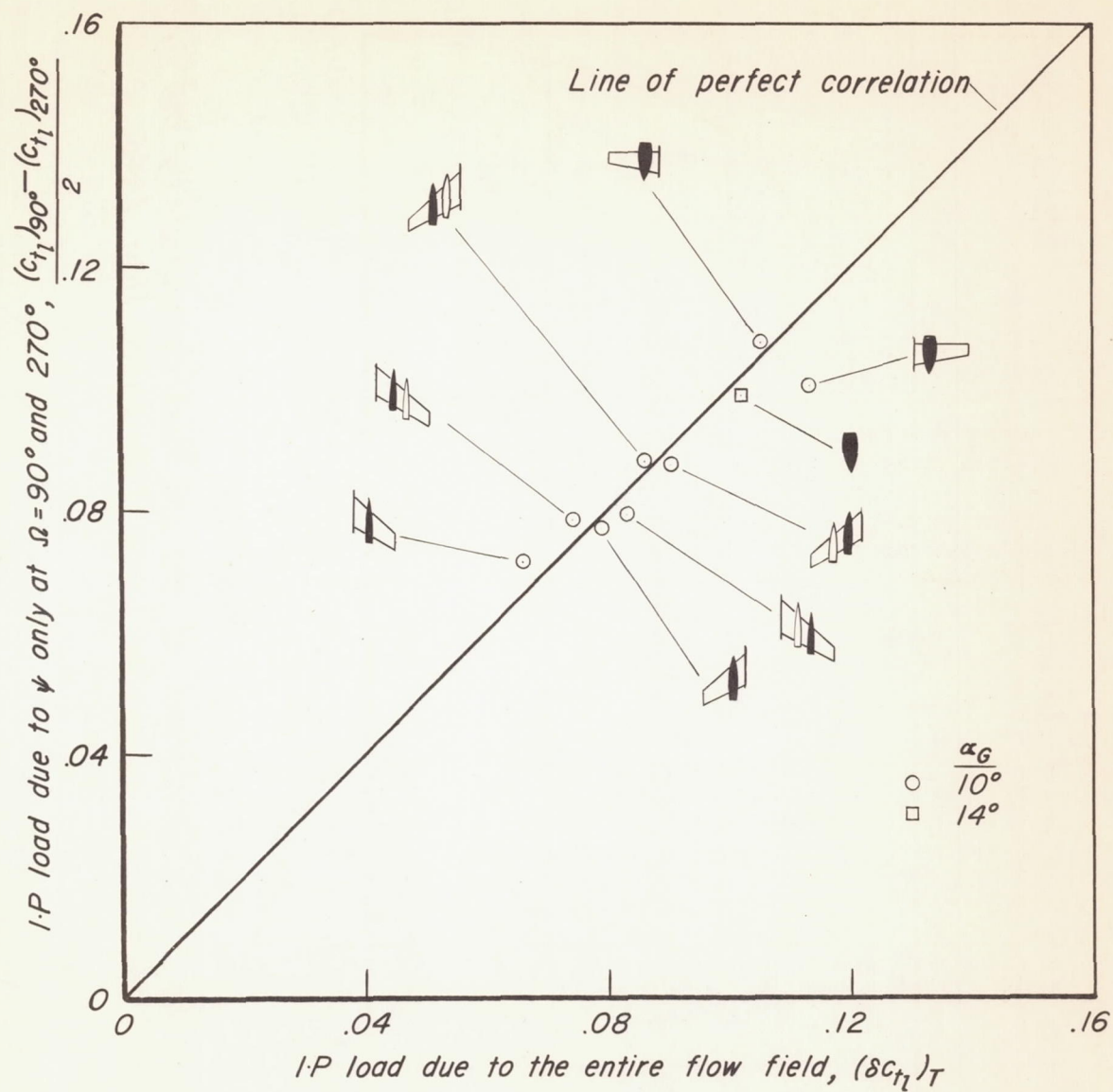
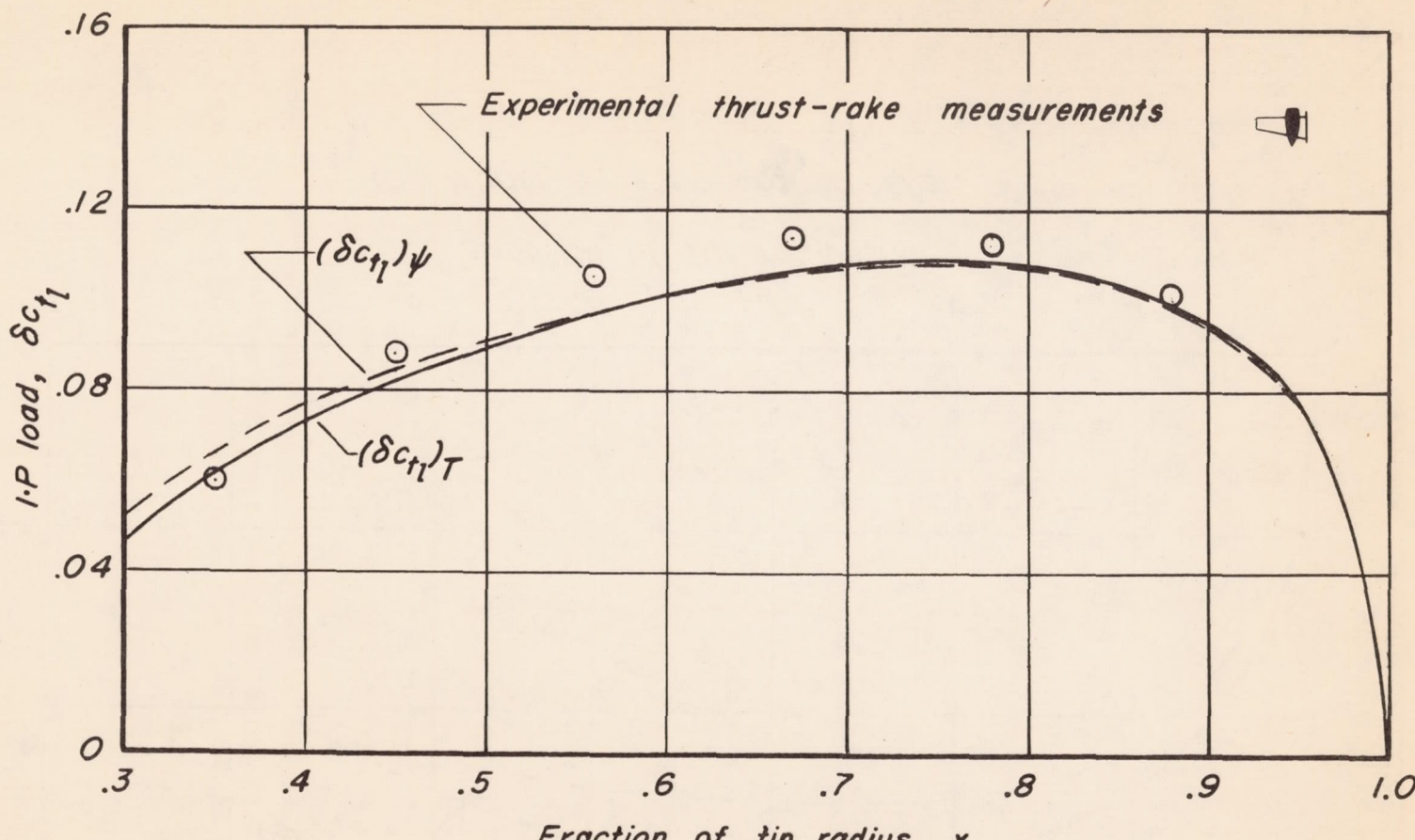
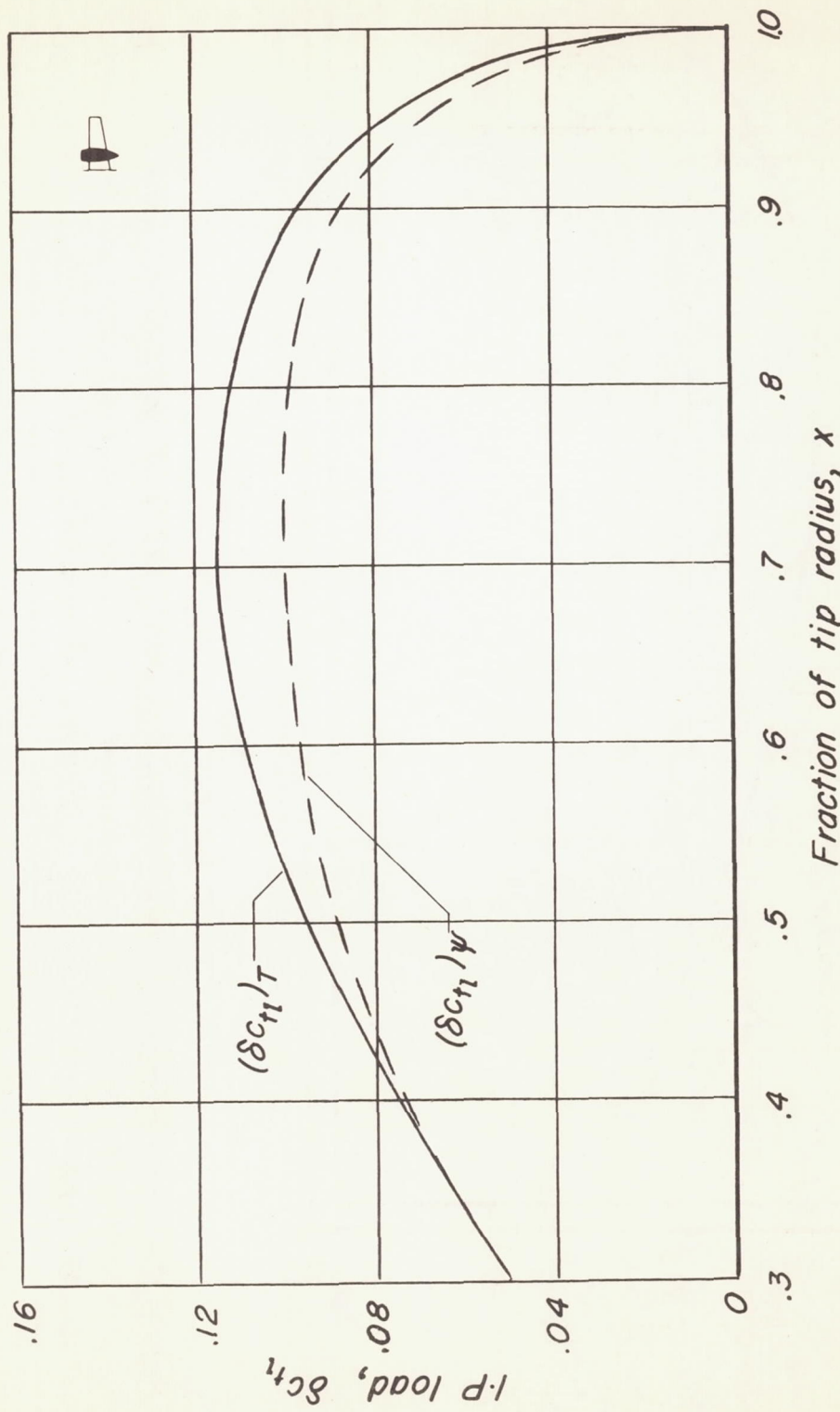


Figure 3.— Comparison of I.P. loads as computed by the procedure of this report with those computed using the entire flow field for several wing-fuselage-nacelle configurations;  $x=0.7$ ,  $V_0=165$  mph,  $n=1250$  rpm,  $\beta_{0.7R}=21.7^\circ$ .



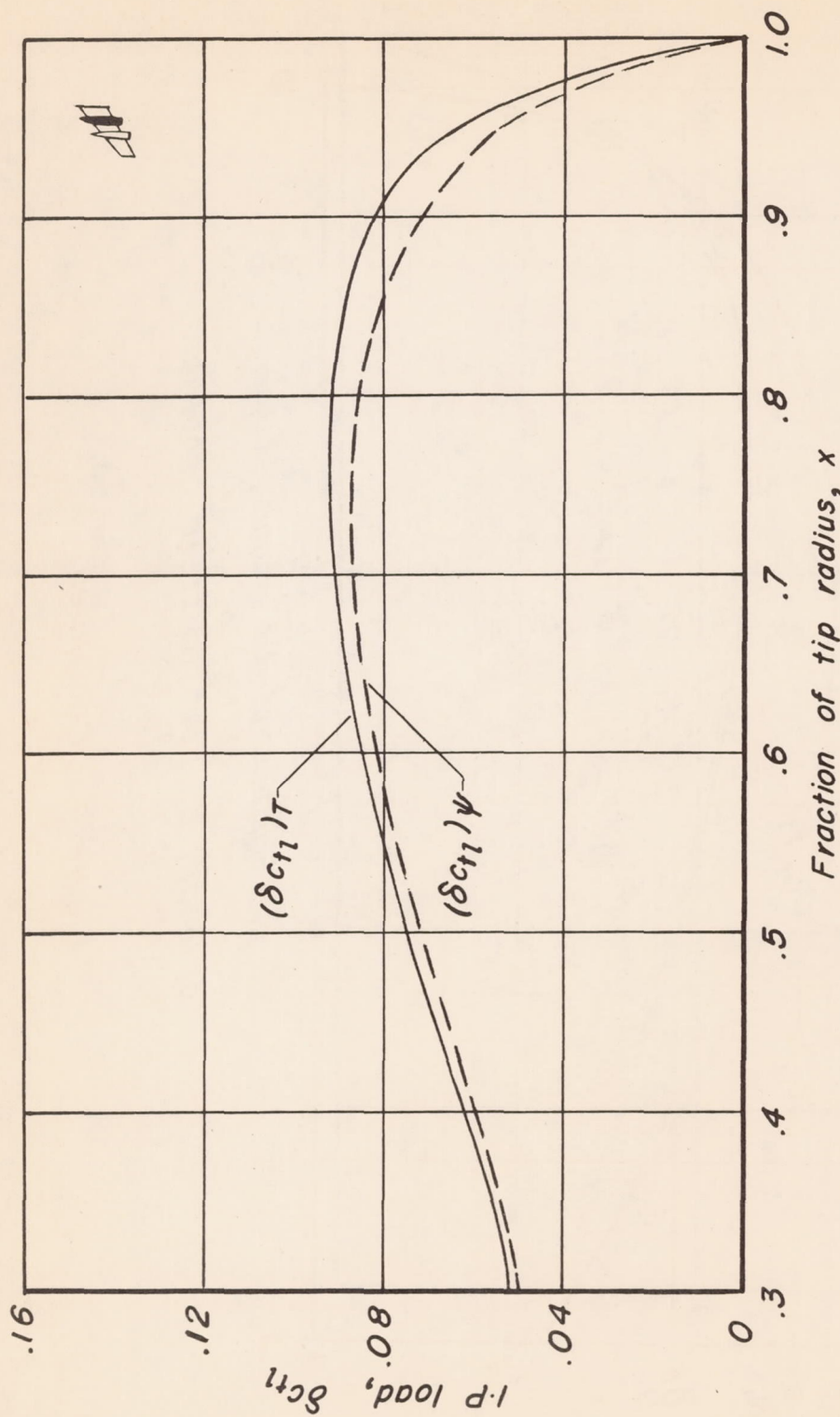
(a) Model b, port propeller.

Figure 4.—Comparison of the radial variation of the I-P load computed by the procedure of this report with that computed using the entire flow field;  
 $V_0 = 165 \text{ mph}$ ,  $n = 1250 \text{ rpm}$ ,  $\beta_{0.7R} = 21.7^\circ$ ,  $\alpha_G = 10^\circ$ .



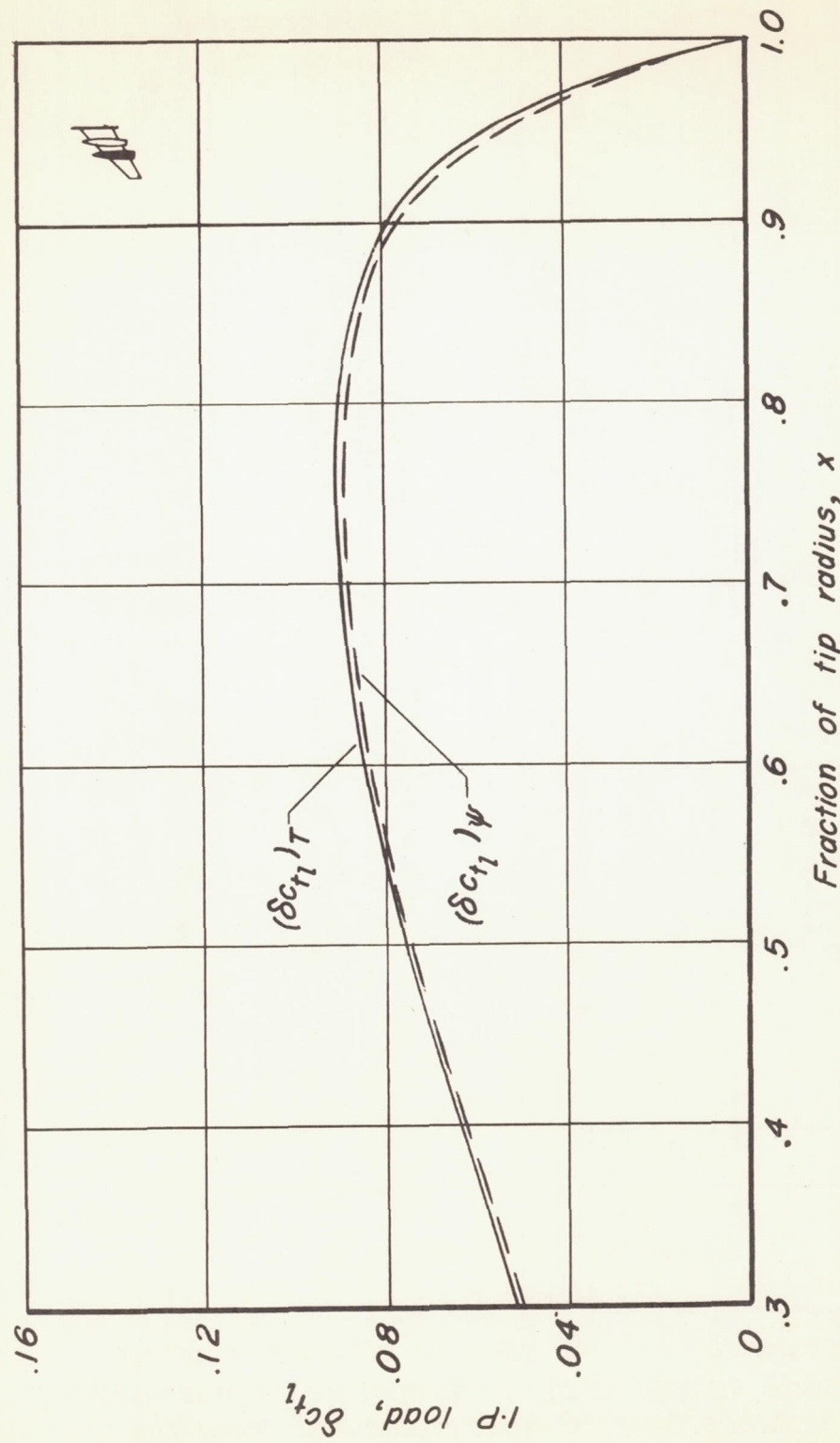
(b) Model b, starboard propeller.

Figure 4.—Continued.



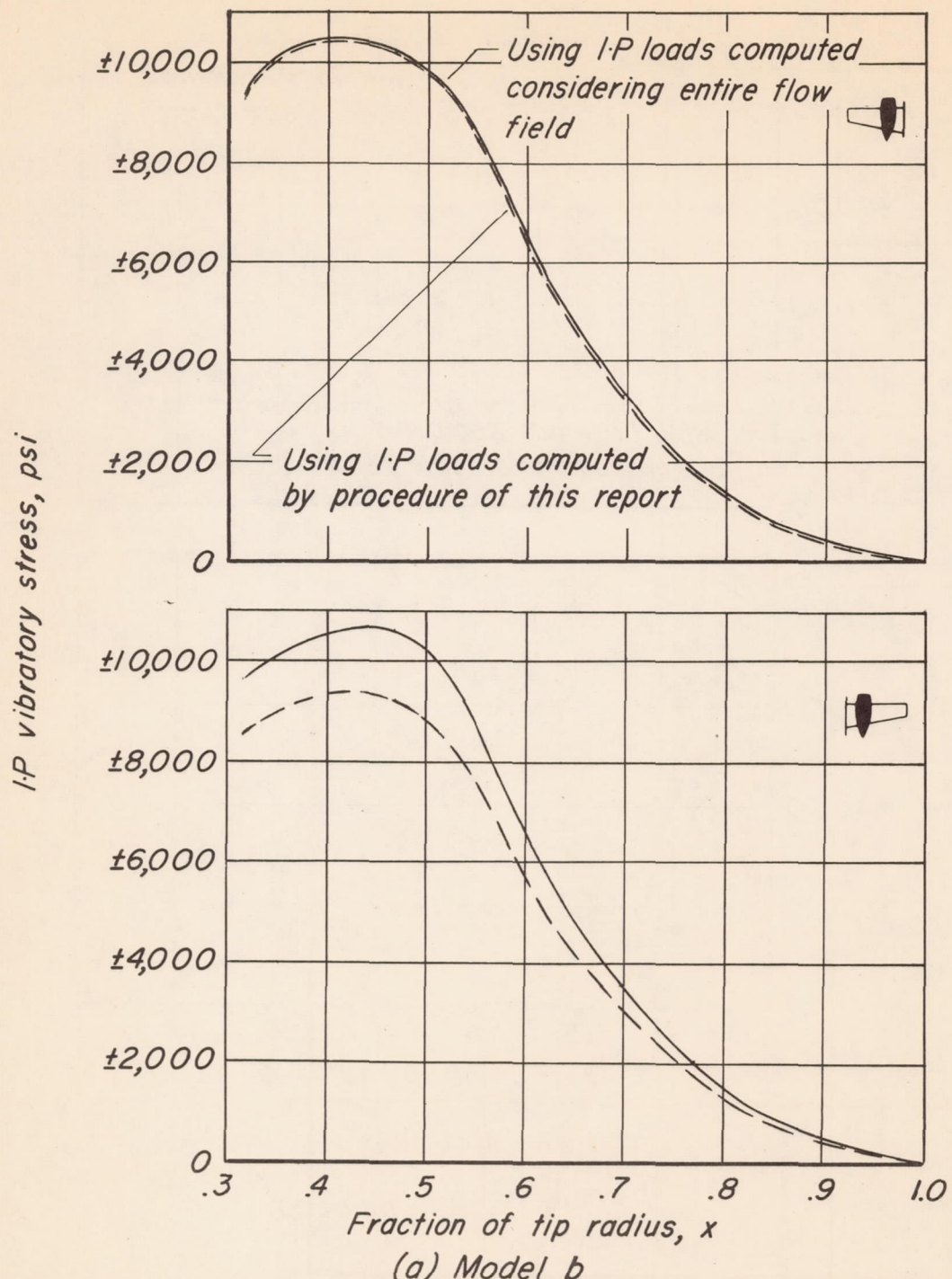
(c) Model c, port inboard propeller.

Figure 4.—Continued.



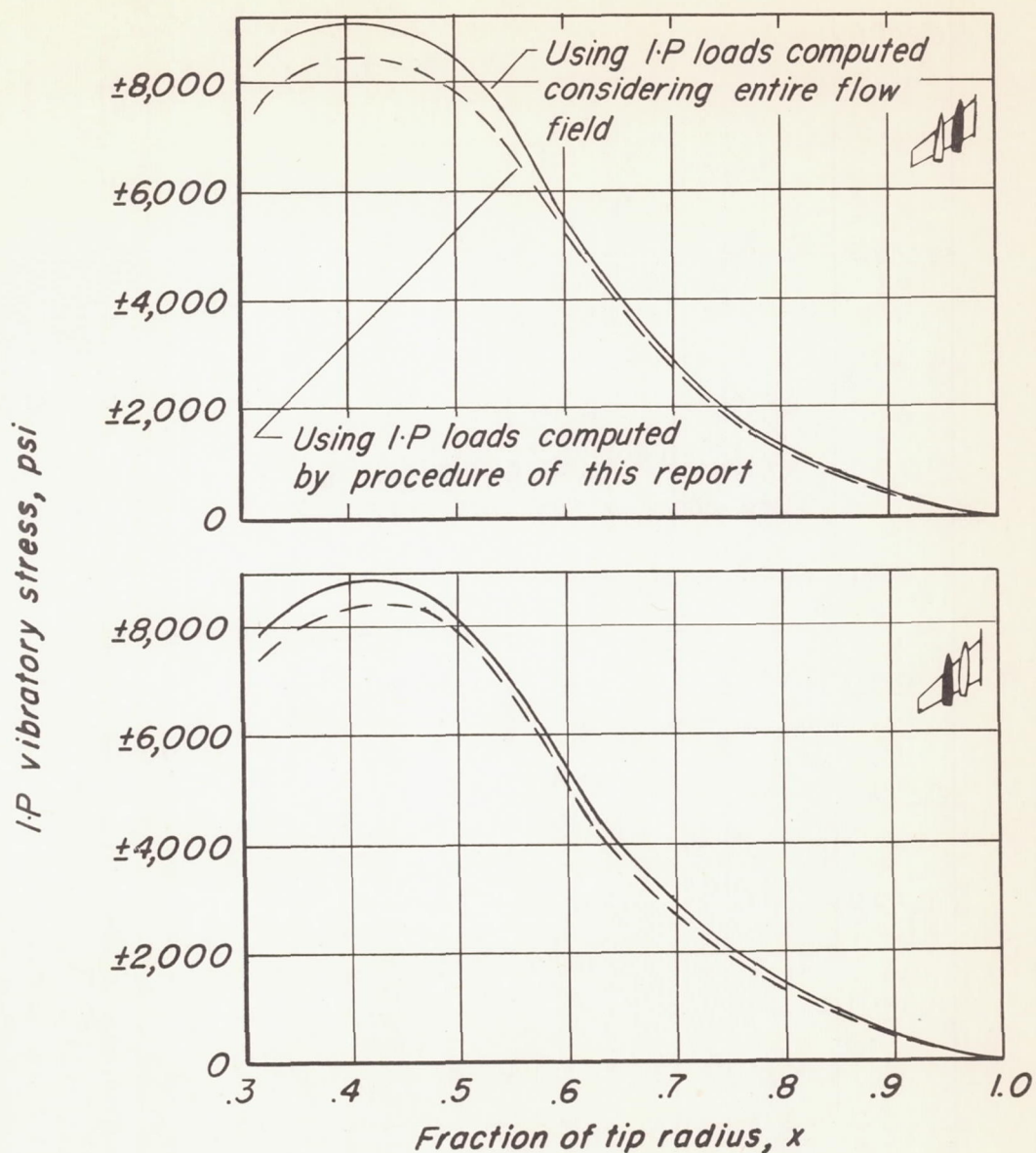
(d) Model c, port outboard propeller.

Figure 4.—Concluded.



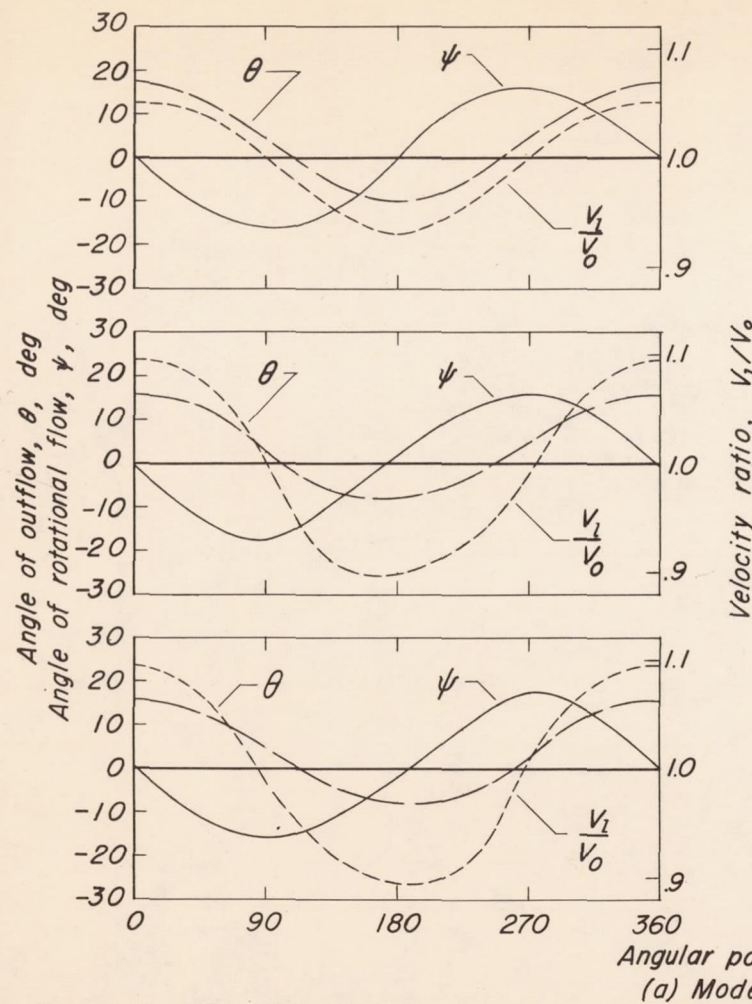
(a) Model b

Figure 5.—Comparison of I-P vibratory stresses resulting from I-P loads computed by the procedure of this report with those resulting from I-P loads computed using the entire flow field;  $V_0=165\text{ mph}$ ,  $n=1250\text{ rpm}$ ,  $\beta_{0.7R}=21.7^\circ$ ,  $\alpha_G=10^\circ$ .



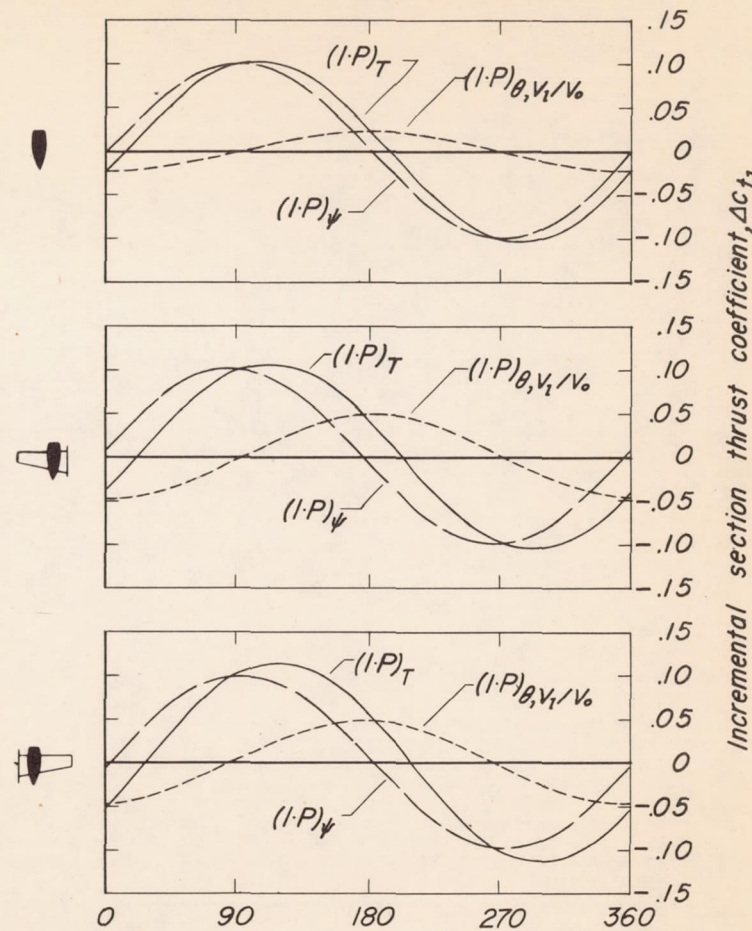
(b) Model c

Figure 5.— Concluded.

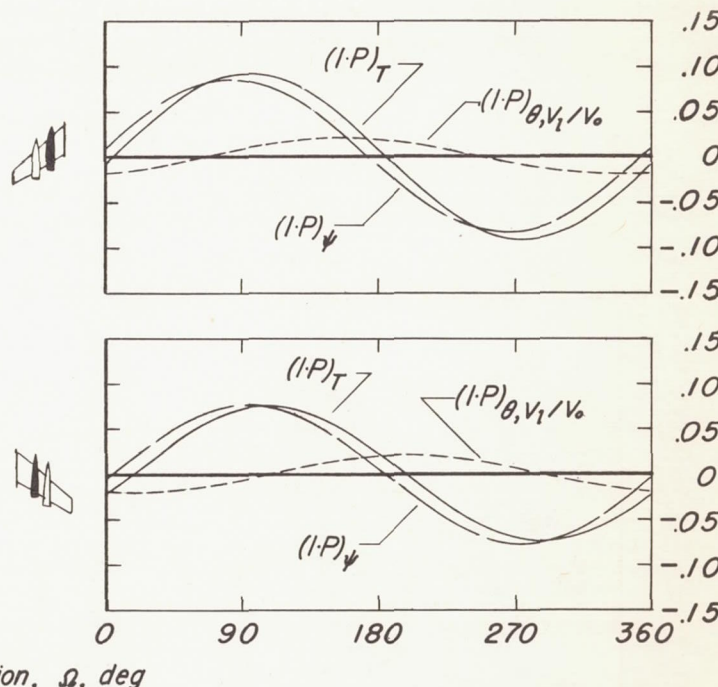


(a) Models a and b

Figure 6.— The flow-field parameters and their effects on the I·P variation of incremental section thrust coefficient for several wing-fuselage-nacelle combinations;  $V_0 = 165$  mph,  $n = 1250$  rpm,  $\beta_{0.7R} = 21.7^\circ$ .

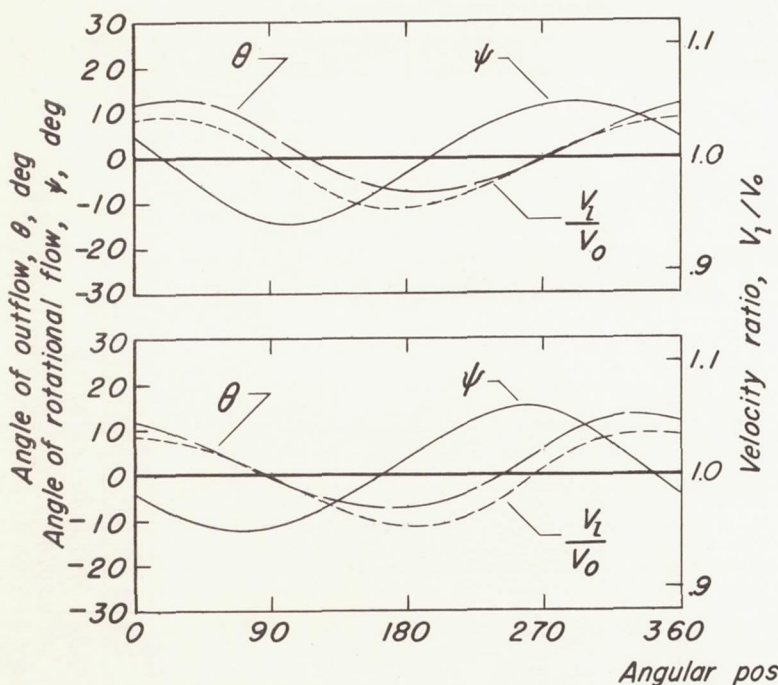


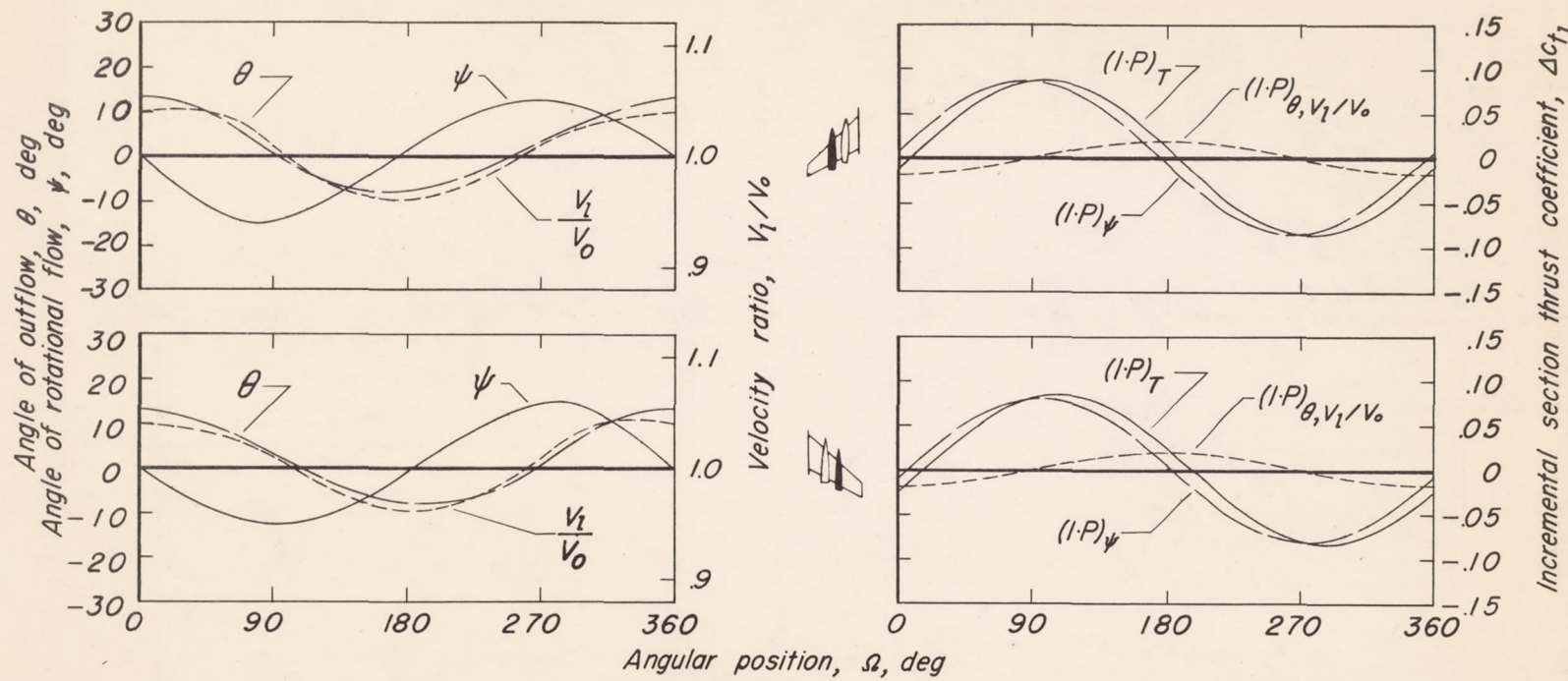
Incremental section thrust coefficient,  $\Delta C_{T_1}$



(b) Model c, inboard

Figure 6.—Continued.





(c) Model c, outboard

Figure 6. — Continued.

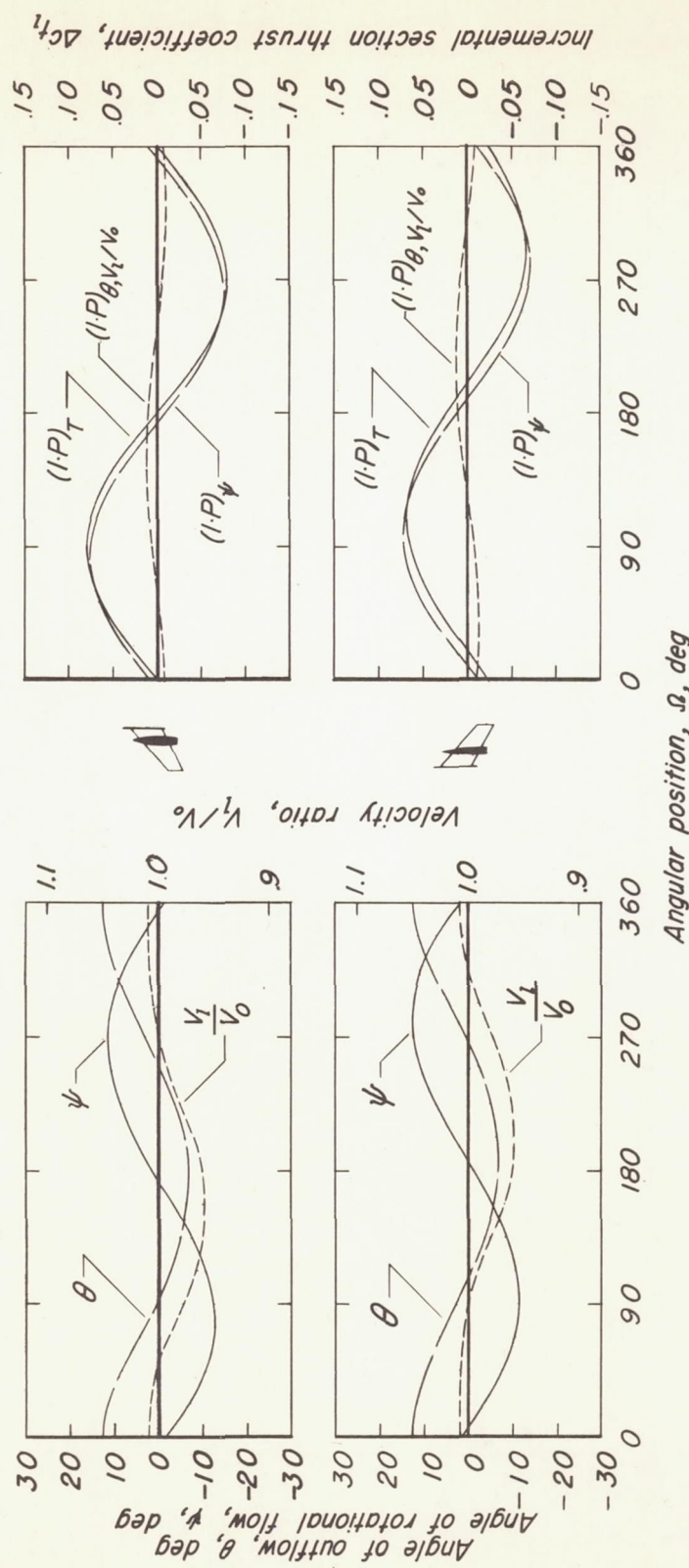


Figure 6.—Concluded.  
(d) Model d